Algebraic Error Analysis for Surface Curvatures of 3-D Range Images

Nabih N. Abdelmalek and Pierre Boulanger

Division of Electrical Engineering
National Research Council of Canada
Ottawa, Ontario, Canada K1A 0R8

ABSTRACT

The method of calculating the Gaussian and mean curvatures of 3-D range images using differential geometry and approximation theory is given. An algebraic error analysis for the calculated curvatures is then presented. Upper bounds for the curvature error terms are obtained as a function of the window size used in the curvature calculation and of the noise standard deviation. The error analysis results are used to illustrate the effect of noise on the segmentation results using curvature sign labels. A segmentation procedure for 3-D range images using a 3-sign label scheme is proposed. Experimental results are presented.

1. INTRODUCTION

Surface curvatures of 3-D range images are invariant under translation and space rotation. They are powerful tools in image description and segmentation.

Normally the range data is contaminated with noise and unfortunately, the calculated surface curvatures for 3-D range images are very sensitive to noise. As a result, when the surface is segmented using the curvature sign labels, spurious patches are created in the segmentation.

In this paper, the method of calculating the surface Gaussian and mean curvatures of 3-D range images using differential geometry and approximation theory is given. The sign label scheme used for segmenting the 3-D range images is explained. An algebraic error analysis for the calculated curvatures is then presented. Upper bounds for the curvature error terms are obtained as a function of the window size used in the curvature calculation and of the noise standard deviation.

The error analysis results are used to illustrate the effect of noise on the segmentation results using curvature sign labels. A practical case shows that the boundaries of the spurious segmentation patches occur where the relative error terms in the calculated curvatures are high. A segmentation procedure for 3-D range images using a 3-sign label scheme is proposed. Experimental results are presented.

2. Gaussian and mean curvatures

At each point on a 3-D surface, there exist a direction of maximum normal curvature denoted by k_1 and an orthogonal direction of minimum normal curvature denoted by k_2. The Gaussian curvature K is defined as the product k_1k_2, while the mean curvature H is the mean $(k_1+k_2)/2$;

$$K = k_1k_2 \quad \text{and} \quad H = (k_1+k_2)/2 \tag{1}$$

Let the range image depth z be defined in terms of the surface coordinates u and v; $z = z(u,v)$. Let also z_u, z_v, z_{uu}, z_{uv} and z_{vv} be the partial derivatives of z with respect to u and v. The curvatures K and H are given by the following formulas [1,2].

$$K = \frac{z_{uu}z_{vv} - z_{uv}^2}{(1 + z_u^2 + z_v^2)^2} \tag{2a}$$

and

$$H = \frac{z_{uu} + z_{vv} + z_{uu}z_v^2 + z_{vv}z_u^2 - 2z_uz_vz_{uv}}{2(1 + z_u^2 + z_v^2)^{1.5}} \tag{2b}$$

In practice, the range image depth z is given in the form of discrete data points at integer (x,y) coordinates. It is common to fit a second degree surface in a least squares sense, to a window centered at each point of the range surface. The partial derivatives of the fitting surface at the centre of the window are taken as the partial derivatives of the range data at that point. The validity of this assumption is not questioned in this work and the results of this paper are based on this assumption.

Figure 1 shows the relative coordinates of the surface points (pixels) inside the 5x5 window and figure 2 shows the pixel labels inside the 5x5 window.

```
        ------- j
        |
        |   (-2,-2) (-2,-1) (-2,0) (-2,1) (-2,2)
        |   (-1,-2) (-1,-1) (-1,0) (-1,1) (-1,2)
      i     (0,-2)  (0,-1)  (0,0)  (0,1)  (0,2)
          (1,-2)  (1,-1)  (1,0)  (1,1)  (1,2)
          (2,-2)  (2,-1)  (2,0)  (2,1)  (2,2)
```

Figure 1. Relative coordinates of the pixels inside a 5x5 window.

1	2	3	4	5
6	7	8	9	10
11	12	13	14	15
16	17	18	19	20
21	22	23	24	25

Figure 2. Pixel labels inside the 5x5 window.

Let the range image depth values inside an LxL window be denoted by z_k, k=1, ..., N, ($N=L^2$), where L is assumed an odd integer and let the fitting second degree surface be

$$z = a_1 + a_2 i + a_3 j + a_4(i^2 - 4) + a_5 ij + a_6(j^2 - 4) \quad (3)$$

where $a_1, \ldots, a_6$ are to be determined.

The set $\{1, i, j, (i^2-4), ij, (j^2-4)\}$ form orthogonal functions over the discrete points such as those shown in figures 1 and 2 [3].

Substituting the pixel coordinates from figures 1 and 2 into equation (3), we get the system of equations

$$\begin{bmatrix} 1 & -2 & -2 & 2 & 4 & 2 \\ 1 & -2 & -1 & 2 & 2 & -1 \\ 1 & -2 & 0 & 2 & 0 & -2 \\ & & & & & \\ . & . & & & & . \\ . & . & & & & . \\ . & . & & & & . \\ & & & & & \\ 1 & 2 & 2 & 2 & 4 & 2 \end{bmatrix} \begin{bmatrix} a_1 \\ a_2 \\ a_3 \\ a_4 \\ a_5 \\ a_6 \end{bmatrix} = \begin{bmatrix} z_1 \\ z_2 \\ z_3 \\ \\ \\ \\ \\ z_{25} \end{bmatrix} \quad (4)$$

which in matrix vector form is

$$Ca = z \quad (5)$$

C is the coefficient matrix in (4), $a=(a_j)$ and $z=(z_i)$.

In the general case, for an LxL window (and M=(L-1)/2), from (3), the columns of the L^2x6 matrix C of equation (4) are given by

Column 1: [1, 1, ..., 1, 1, 1 (L^2 times)]. (6a)

Column 2: [(-M (L times), -(M-1) (L times),..., -1 (L times), 0 (L times), 1 (L times), ..., (M-1) (L times), M (L times)] (6b)

Column 3: [(-M, -(M-1), ..., -1, 0, 1, ..., (M-1), M) (L times)]. (6c)

Column 4: [($(M^2-M(M+1)/3)$ (L times), $((M-1)^2 - M(M+1)/3)$ (L times), ..., (1-M(M+1)/3) (L times), -M(M+1)/3 (L times), (1-M(M+1)/3) (L times), ..., $((M-1)^2-M(M+1)/3)$ (L times), $(M^2-M(M+1)/3)$ (L times)] (6d)

Column 5: The jth element of column 5 is the product of the jth element of column 2 and the jth element of column 3. (6e)

Column 6: [($(M^2-M(M+1)/3)$, $((M-1)^2-M(M+1)/3)$, .., (1-M(M+1)/3), -M(M+1)/3, (1-M(M+1)/3),..., $((M-1)^2-M(M+1)/3)$, $(M^2-M(M+1)/3)$) (L times)]. (6f)

The solution vector 'a' in the least squares sense of equation (5), is the solution of the normal equation of equation (5). See for example Stewart [4]. This normal equation is obtained by premultiplying (5) by C^T, the transpose of matrix C. That is

$$C^T Ca = C^T z \quad (7)$$

From matrix C defined in equation (4), the normal equation (7) is

$$\begin{bmatrix} 25 & 0 & 0 & 0 & 0 & 0 \\ 0 & 50 & 0 & 0 & 0 & 0 \\ 0 & 0 & 50 & 0 & 0 & 0 \\ 0 & 0 & 0 & 70 & 0 & 0 \\ 0 & 0 & 0 & 0 & 100 & 0 \\ 0 & 0 & 0 & 0 & 0 & 70 \end{bmatrix} \begin{bmatrix} a_1 \\ a_2 \\ a_3 \\ a_4 \\ a_5 \\ a_6 \end{bmatrix} = \begin{bmatrix} z_a \\ z_b \\ z_c \\ z_d \\ z_e \\ z_f \end{bmatrix} \quad (8)$$

In the general case for an LxL window and again M=(L-1)/2, equation (8) is given by

$$\begin{bmatrix} A & 0 & 0 & 0 & 0 & 0 \\ 0 & B & 0 & 0 & 0 & 0 \\ 0 & 0 & B & 0 & 0 & 0 \\ 0 & 0 & 0 & C & 0 & 0 \\ 0 & 0 & 0 & 0 & D & 0 \\ 0 & 0 & 0 & 0 & 0 & C \end{bmatrix} \begin{bmatrix} a_1 \\ a_2 \\ a_3 \\ a_4 \\ a_5 \\ a_6 \end{bmatrix} = \begin{bmatrix} z_a \\ z_b \\ z_c \\ z_d \\ z_e \\ z_f \end{bmatrix} \quad (9)$$

The elements of the r.h.s. vector ($z_a, \ldots, z_f$) are the scalar products of vector z of equation (5) with the columns of matrix C. Also from (7) and (6) the diagonal elements of the coefficient matrix in (9) are

$$\begin{aligned} A &= L^2 \\ B &= M(M+1)L^2/3 \\ C &= M(M+1)(4M^2+4M-3)L^2/45 \\ D &= M^2(M+1)^2L^2/9 \end{aligned} \quad (10)$$

For the summation of series see Jolley [5].

From (9) the unknown elements ($a_1, \ldots, a_6$) are given by

$$\begin{aligned} &a_1 = z_a/A, \quad a_2 = z_b/B, \quad a_3 = z_c/B, \\ &a_4 = z_d/C, \quad a_5 = z_e/D, \quad a_6 = z_f/C \end{aligned} \quad (11)$$

From equation (3) the partial derivatives z_u, ..., z_{vv} at the centre of the window (0,0) are given by

$$z_u = a_2, \; z_v = a_3, \; z_{uu} = 2a_4, \; z_{uv} = a_5, \; z_{vv} = 2a_6 \quad (12)$$

These are taken as the partial derivatives at the object surface point upon which the window is centered.

2.1 Surface curvature sign labeling

Besl and Jain [2,6], used an 8 sign labeling scheme for range image surfaces. At each point on the image surface the sign of the Gaussian and mean curvatures are recorded; >0, =0 or <0. Hence we have 9 combinations, of which one is not possible. This is for H=0 and K>0, since in this case from (1), $k_1 = -k_2$ and $K = k_1 k_2$ cannot be >0. When this labeling scheme is done, the boundaries of different patches are determined. This gives a coarse image segmentation.

3. ALGEBRAIC ERROR ANALYSIS FOR SURFACE CURVATURES

We assume that the noise contaminating a given range data is of zero mean and has normal (Gaussian) distribution of standard deviation σ. In this case the amplitude of over 95% of the noise is $\leq 2\sigma$.

The error terms in the calculated surface curvatures are obtained by applying techniques similar to those used for roundoff error analysis in algebraic processes [7].

3.1 Error bounds in the calculated $(\bar{z}_a, \ldots, \bar{z}_f)$

Let the exact image depth in the LxL window be z_i and the noise in the measured depth be δ_i and let the measured parameters be denoted by lower bars. Then

$$\underline{z}_i = z_i + \delta_i, \qquad \text{where} \qquad |\delta_i| \leq 2\sigma. \tag{13}$$

Let the calculated parameters be denoted by upper bars. The calculated elements $(\bar{z}_a, \ldots, \bar{z}_f)$ of the r.h.s. vector of equation (9) are obtained as follows.

From (6a) and (13)

$$\bar{z}_a = \sum_1^{L^2} \underline{z}_i = \sum_1^{L^2} (z_i + \delta_i) = z_a + E_a$$

E_a is the error term in the calculated $\bar{z}_a$ and is given by

$$E_a = \sum_1^{L^2} \delta_i$$

Hence

$$|E_a| = |\sum_1^{L^2} \delta_i| \leq \sum_1^{L^2} |\delta_i| \leq 2L^2\sigma \tag{14a}$$

From (6b) and (13)

$$\bar{z}_b = -M\sum_1^{L} \underline{z}_i - (M-1)\sum_{L+1}^{2L} \underline{z}_i - \ldots - \sum_{(M-1)L+1}^{ML} \underline{z}_i + \sum_{(M+1)L+1}^{(M+2)L} \underline{z}_i + \ldots + M\sum_{(L-1)L+1}^{L^2} \underline{z}_i$$

$$= z_b + E_b$$

where

$$E_b = -M\sum_1^{L} \delta_i - (M-1)\sum_{L+1}^{2L} \delta_i - \ldots - \sum_{(M-1)L+1}^{ML} \delta_i + \sum_{(M+1)L+1}^{(M+2)L} \delta_i + \ldots + M\sum_{(L-1)L+1}^{L^2} \delta_i$$

Hence

$$|E_b| \leq |-M\sum_1^{L} \delta_i| + |-(M-1)\sum_{L+1}^{2L} \delta_i| + \ldots + |-\sum_{(M-1)L+1}^{ML} \delta_i| + |\sum_{(M+1)L+1}^{(M+2)L} \delta_i| + \ldots + |M\sum_{(L-1)L+1}^{L^2} \delta_i|$$

$$\leq M\sum_1^{L} |\delta_i| + (M-1)\sum_{L+1}^{2L} |\delta_i| + \ldots + \sum_{(M-1)L+1}^{ML} |\delta_i| + \sum_{(M+1)L+1}^{(M+2)L} |\delta_i| + \ldots + M\sum_{(L-1)L+1}^{L^2} |\delta_i|$$

$$\leq L[M+(M-1)+ \ldots +1+1+ \ldots +(M-1)+M]2\sigma$$

$$= 2LM(M+1)\sigma. \tag{14b}$$

In a similar manner from (6c) and (13)

$$|E_c| \leq 2LM(M+1)\sigma. \tag{14c}$$

Again using algebraic manipulation we get

$$|E_d| \leq 0.7L\,M(M+1) \tag{14d}$$

$$|E_f| \leq 0.7L\,M(M+1) \tag{14e}$$

and finally from (6b), (6c) and (13), we get

$$|E_e| \leq 2M^2(M+1)^2\sigma \tag{14f}$$

3.2 Error bounds in the calculated partial derivatives $(\bar{z}_u, \ldots, \bar{z}_{vv})$

Let the calculated partial derivatives be given by

$$\bar{z}_u = z_u + E_u, \quad \bar{z}_v = z_v + E_v, \quad \ldots, \quad \bar{z}_{vv} = z_{vv} + E_{vv} \tag{15}$$

where $E_u, \ldots, E_{vv}$ are their respective errors.

From (12), (11) and (10),

$$E_u = E_b/B, \quad E_v = E_c/B, \quad E_{uu} = 2E_d/C, \quad E_{uv} = E_e/D, \quad E_{vv} = 2E_f/C \tag{16}$$

Hence from (14), (10) and (16), we get

$$\begin{aligned} |E_u| &\leq 6\sigma/L \\ |E_v| &\leq 6\sigma/L \\ |E_{uu}| &\leq 63\sigma/(L^2-4) \\ |E_{uv}| &\leq 18\sigma/L^2 \\ |E_{vv}| &\leq 63\sigma/(L^2-4) \end{aligned} \tag{17}$$

3.3 Error bounds in the calculated Gaussian curvature $\bar{K}$

Substituting (15) into (2a), the calculated value of K is given by

$$\bar{K} = \frac{(z_{uu}+E_{uu})(z_{vv}+E_{vv}) - (z_{uv}+E_{uv})^2}{[1+(z_u+E_u)^2+(z_v+E_v)^2]^2} \tag{18}$$

After neglecting second order error terms and after some algebraic manipulation, we write

$$\bar{K} = K[1 + \delta_K] \tag{19a}$$

where

$$|\delta_K| \leq \left[\frac{(63\alpha|z_{uu}|+63\alpha|z_{vv}|+36|z_{uv}|)(24|z_u|+24|z_v|)}{|(z_{uu}z_{vv}-z_{uv}^2)|L^2} + \frac{}{(1+z_u^2+z_v^2)L}\right]\sigma \tag{19b}$$

In (19b) we have replaced the factor $1/(L^2-4)$ of (17) by the factor α/L^2, where $\alpha < 1.2$ for window size $L \geq 5$.

We may write (19a) differently,

$$\bar{K} = K + E_K \tag{20}$$

where

$$E_K = K\,\delta_K \tag{20a}$$

and hence

$$|E_K| \leq \left[\frac{63\alpha(|z_{uu}|+|z_{vv}|)+36|z_{uv}|}{(1+z_u^2+z_v^2)^2L^2} + \frac{24(|z_u|+z_v|)}{(1+z_u^2+z_v^2)L}|K|\right]\sigma \tag{20b}$$

3.4 Error bounds in the calculated mean curvature $\bar{H}$

Substituting (15) into (2b) and following the same steps for calculating E_K, we get

$$\bar{H} = H[1 + \delta_H] \tag{21a}$$

where after algebraic manipulation

$$|\delta_H| \le [\frac{63\alpha(2+z_u^2+z_v^2)+36|z_u z_v|+12(|z_v z_{uu}|+|z_u z_{vv}|+|z_u z_{uv}|+|z_v z_{uv}|)L}{|z_{uu}(1+z_v^2)+z_{vv}(1+z_u^2)-2z_u z_v z_{uv})L} + \frac{18(|z_u|+|z_v|}{(1+z_u^2+z_v^2)L}]\sigma \tag{21b}$$

Again we may write (21a) differently;

$$\bar{H} = H + E_H \tag{22}$$

where

$$E_H = H\,\delta_H \tag{22a}$$

and hence

$$|E_H| \le [\frac{63\ (2+z_u^2+z_v^2)+36|z_u z_v|+12(|z_v z_{uu}|+|z_u z_{vv}|+|z_u z_{uv}|+|z_v z_{uv}|)L}{(1+z_u^2+z_v^2)^{1.5}\ L^2} + \frac{18(|z_u|+|z_v|)}{(1+z_u^2+z_v^2)L}|H|]\sigma \tag{22b}$$

3.5 More realistic error upper bounds for K and H

The r.h.s. of (20b) and (22b) give the error upper bounds of $|E_K|$ and $|E_H|$ respectively. In obtaining these upper bounds, the signs and amplitudes of the individual error terms are taken in such a way as to give the largest possible bounds for $|E_K|$ and $|E_H|$. These upper bounds are hardly likely to be attained.

In estimating the rounding errors for the Gauss LU decomposition method and for other algebraic methods, Wilkinson ([7], pp. 25-26, 102, 52) obtained upper bounds which are also unrealistic. Using statistical arguments, backed with numerical experience, Wilkinson stated that even the replacement of a factor like the factors between square brackets in (20b) and (22b) by their square roots give overestimates to the true upper bounds. Hence we here replace (20b) and (22b) respectively by

$$|E_K| \le \Theta_K \sigma \tag{23a}$$

$$|E_H| \le \Theta_H \sigma \tag{23b}$$

where Θ_K and Θ_H are the square root of the coeficients in square brackets in (20b) and (22b) respectively.

Once more from (20a) and (22a), δ_K and δ_H are given by

$$|\delta_K| \le \Theta_K \sigma / |K| \tag{24a}$$

$$|\delta_H| \le \Theta_H \sigma / |H| \tag{24b}$$

where each of K and H is assumed nonzero. Again δ_K and δ_H are the relative error terms for K and H respectively.

3.6 The effect of noise on the segmentation results

Let us consider the curvature relative error terms of (19a) and (21a). If in (19a) the relative error term δ_K is <-1, the square bracket in (19a) becomes negative and the calculated $\bar{K}$ will have the opposite sign of the real K. This case is more likely to happen for very small values of K. Since from (2a) for very small values of K, $(\bar{z}_{uu}\bar{z}_{vv}-\bar{z}_{uv}^2)$ would be very small and possibly with the wrong sign. The first term on the r.h.s of (19b) would then be very large and with the wrong sign, making K very susceptible to noise. Similar argument could be drawn from (21a) and (21b) for the relative error term of the mean curvature H.

We now illustrate the effect of noise on the segmentation results using curvature sign labels on a practical example. See also section 4 below.

The upper bounds of the curvature relative error terms, the r.h.s. of (24a) and (24b) are calculated for the image surface points. The calculated values are displayed in the form of contour maps. The contours in each map are shown at equal intervals and are labeled as (0123456789abc ... wxyz0123 ... wxyz ...) in ascending order.

Figure 3 shows the image of the 'Grapper fixture' . The round base is a flat surface which has K=H=0 at each point except where the 3 wings are attached. Therefore any segmentation of this flat surface is spurious. Figure 4 shows the jump edges in figure 3.

Figure 5 shows the segmented image where the '+' symbols are the boundaries obtained from the 8-sign label scheme of the curvatures K and H [2].

Figure 6 shows the contour map for the r.h.s. of (24a) for K. The ' ' symbols are the image background, the pixels where $|K| <$ EpsK (a small tolerence for K) or the pixels where this r.h.s. is very large. The '.' symbols are the boundaries of the segmentation patches in figure 5. Figure 7 shows the same for H.

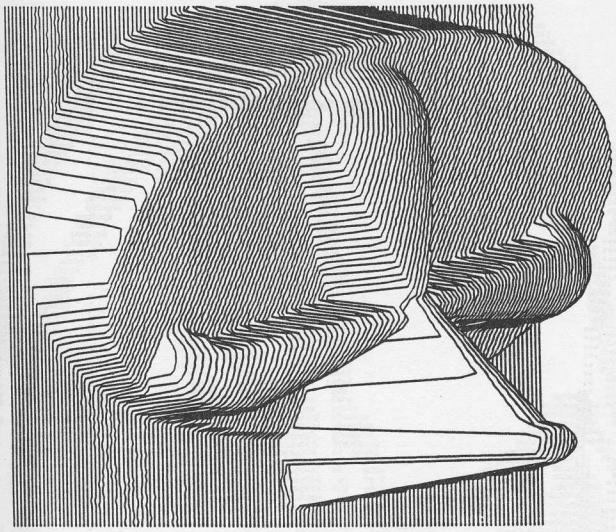

Figure 3: The 'Grapper fixture'.

From figures 6 and 7 the boundaries of the spurious segmentation patches occur where either the relative error terms of K are high or where those of H are high.

4. PROPOSED SEGMENTATION PROCEDURE

In our proposed segmentation procedure the image surface is segmented using the 3 sign labels of H only. The jump edges are then imposed on the segmented image. Further, the boundary points between adjacent surface patches are examined for the purpose of keeping or removing them. A boundary point which is not on a jump edge, has to belong to a crease or to a ridge line. These steps are now briefly outlined.

4.1 Segmentation using 3-sign label scheme

In this scheme, a range surface point belongs to a convex, a concave or a flat patch only. The sign of H is itself the sign of the maximum (in absolute value) of the normal curvature k_1 or k_2. Hence we assume that a convex patch has $H>0$ for all K; <0, $=0$ or >0. We also assume that a concave patch has $H<0$ for all K. A flat patch has $H=K=0$. There remains one case; for $H=0$ and $K<0$, which is for $k_1=-k_2$, known as the minimum saddle case. This case may be considered by itself, if it ever occurs.

4.2 The surface jump edges

At jump edges the surface undergoes discontinuities. We here detect jump edges by using the 3x3 Sobel edge operator [8] with a suitable threshold level. A main reason for calculating the jump edges and imposing them over the curvature-segmented image is that computing curvatures in the vicinity of jump edges can give meaningless results [9]

4.3 Detection of creases and ridges

Folds or creases in range images correspond to surface normal discontinuities and ridge lines correspond to discontinuities of curvatures. A boundary point between patches which is not on a jump edge is tested. If it is not a crease or a ridge point, this point is deleted. Such crease and ridge points are detected by the existence of large residual norms for the approximating planes on the windows centered at the tested points. If the residual norm is less than a certain threshold, the point is deleted.

4.4 Results for the proposed segmentation procedure

Figure 8 shows the segmented image of our scheme. The '+' symbols are the boundaries obtained from the proposed 3-sign label scheme. Figure 9 shows the final segmentation for figure 3, which is very close to figure 4. Our experimental results show that the 3-sign label scheme gives better results than those obtained from the 8-sign label scheme.

5. COMMENTS AND CONCLUSION

In the literature, most papers dealing with 3-D range images calculate the surface curvatures in a similar way to that described in section 2 above. If the method of calculating the surface curvatures is different from that described here, the error analysis will differ accordingly and the upper bounds of the curvature error terms will be different from those obtained here.

REFERENCES

1. E. Kreyszig, Introduction to Differential Geometry and Riemannian Geometry, University of Toronto Press (1968).
2. P.J. Besl and R. Jain, Invariant surface characteristics for 3D object recognition in range images, Computer Vision, Graphics and Image Processing, 33, 33-80 (1986).
3. R.M. Haralick, Digital step edges from zero crossing of second directional derivatives, IEEE Trans. Pattern Analysis and Machine Intelligence, PAMI-6, 58-68 (1984).
4. G.W. Stewart, Introduction to Matrix Computation, Academic Press, New York (1973).
5. L.B.Jolley, Summation of Series, Dover Publications, New York (1963).
6. P.J. Besl and R. Jain, Segmentation through variable order surface fitting, IEEE Trans. Pattern Analysis and Machine Intelligence, PAMI-10, 167-192 (1988).
7. J.H. Wilkinson, Rounding Error in Algebraic Processes, Prentice-Hall, Englewood Cliffs, N.J. (1963).
8. E.L. Hall, Computer Image Processing and Recognition, Academic Press, New York (1979).
9. B.C. Vemuri, A. Mitiche J.K. Aggarawal,J.K., in Three Dimensional Machine Vision, Kanada, T. (Ed.), pp. 241-266, Kluwer Academic Publishers, Boston, Mass. (1987).

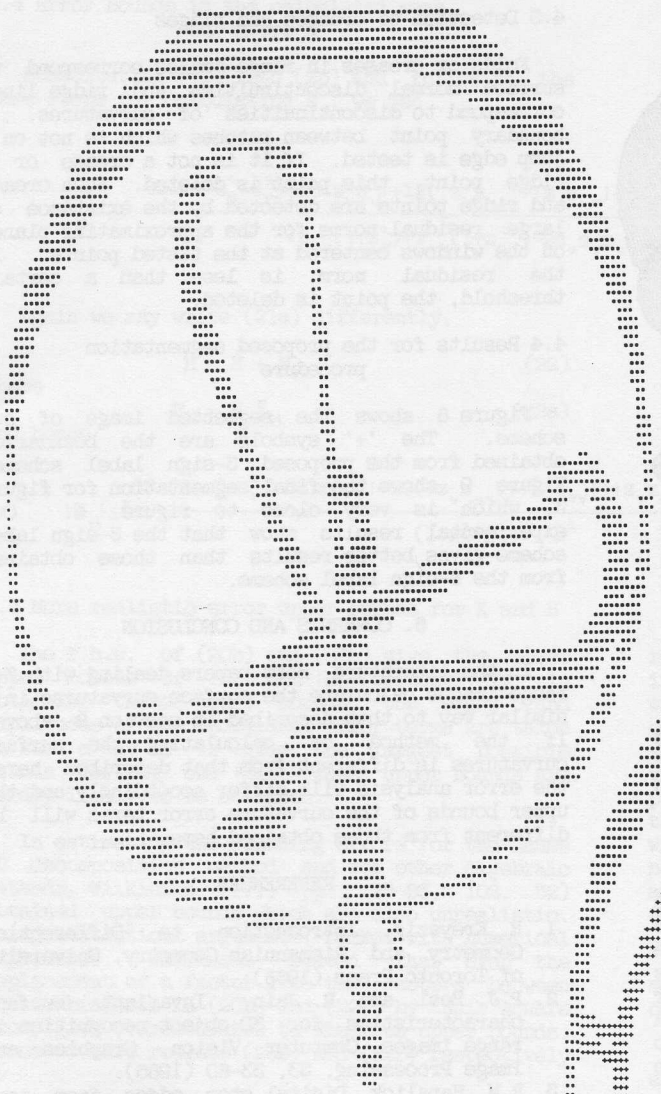

Figure 4: The jump edges in figure 3.

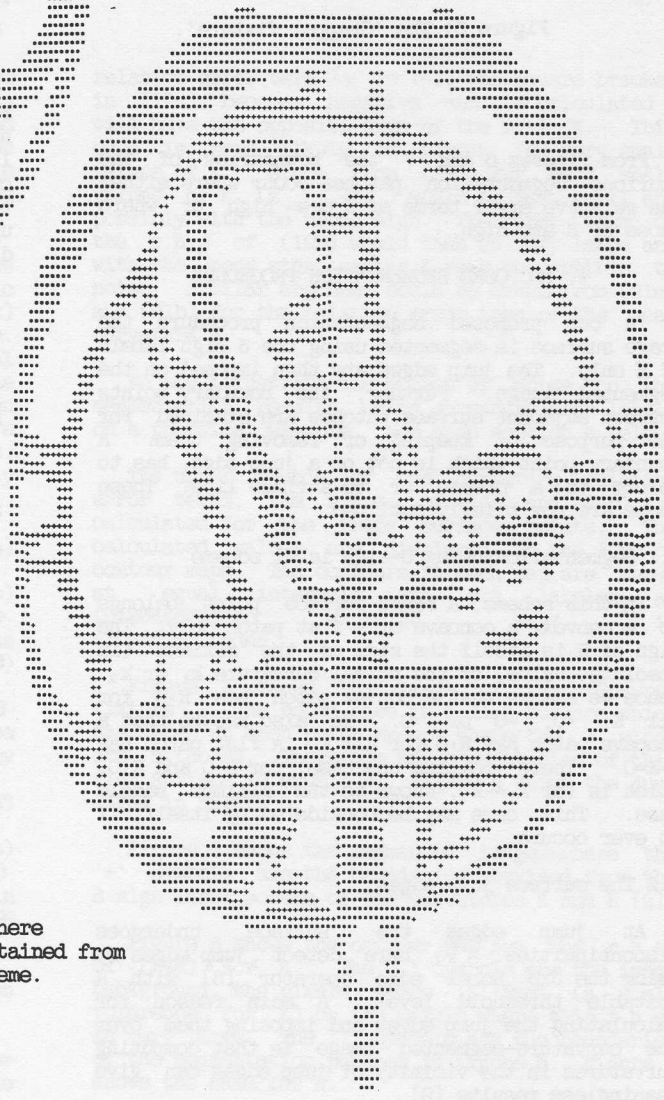

Figure 5: The segmented image where the '+' symbols are the boundaries obtained from the 8-sign curvature label scheme.

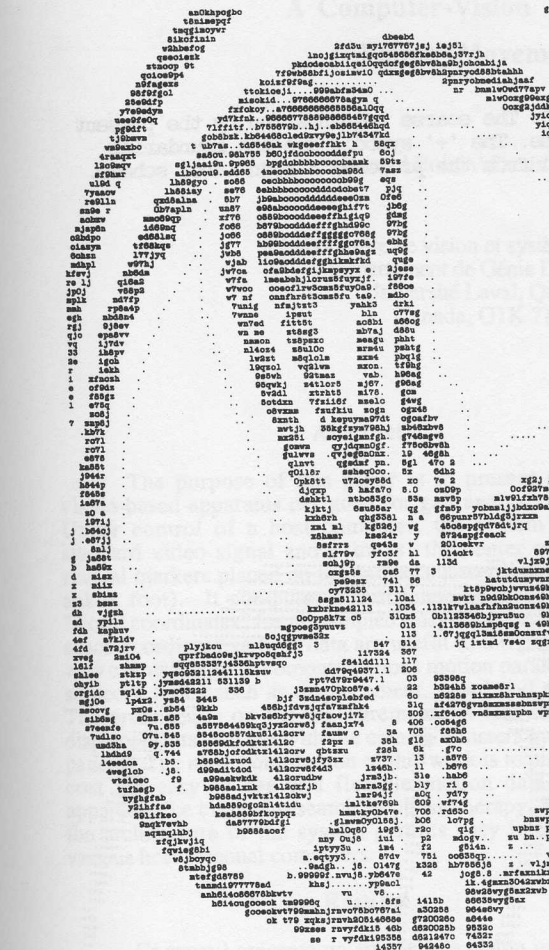

Figure 7: Same as figure 6, but for the mean curvature H.

Figure 6: The contour map for the relative error terms of the Gaussian curvature K. The ' ' symbols are the image background, the pixels where $|K| < EpsK$, or the pixels where $|\delta_K|$ is very large. The '.' symbols are the boundaries of the segmentation patches in figure 5.

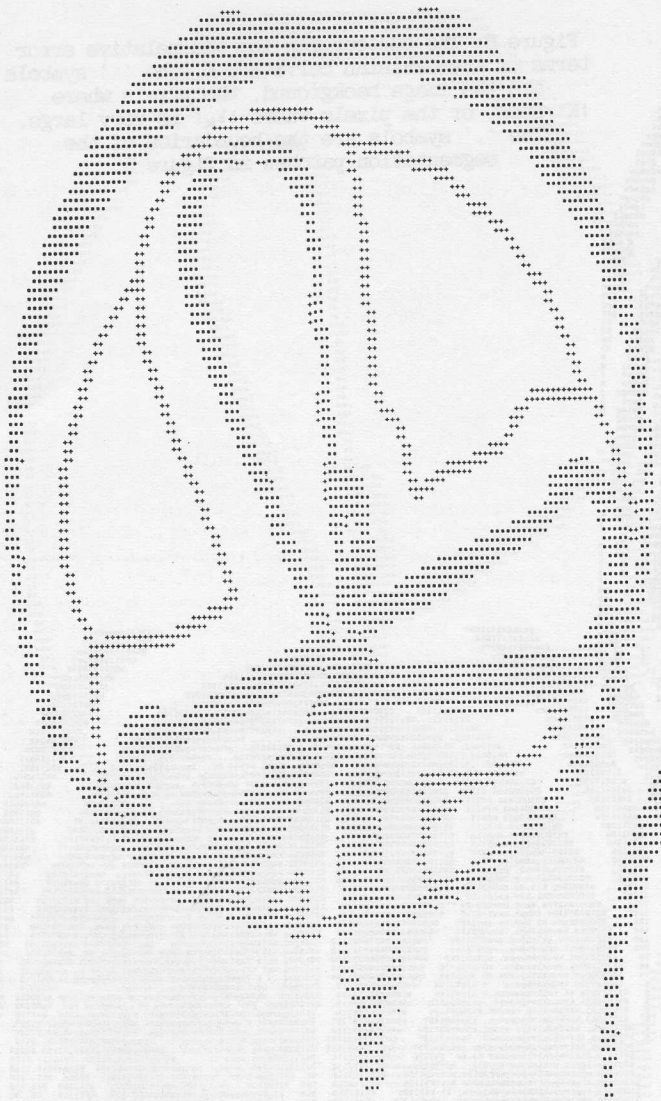

Figure 8: The coarse segmentation by the present scheme. The '+' symbols are the boundaries obtained from the proposed 3-sign label scheme.

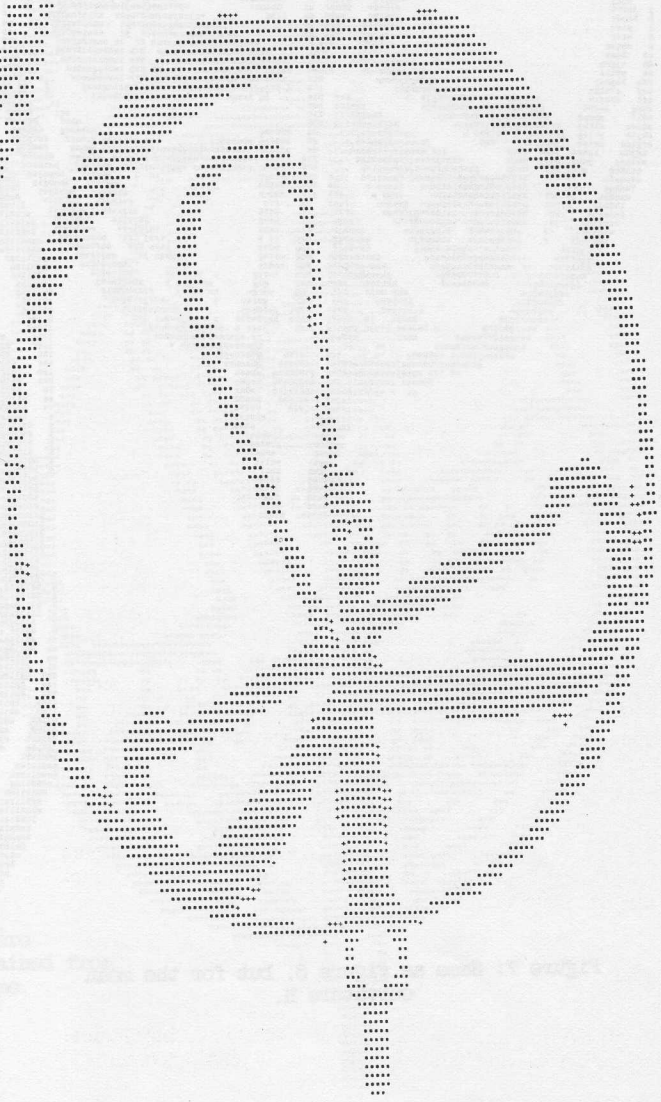

Figure 9: The final segmentation of the range image of figure 3.